

Long Period, Long Duration (LPLD) Seismicity and their Probable Role in Reservoir Stimulation and Stage Productivity

Abhash Kumar, AECOM, National Energy Technology Laboratory; **Erich Zorn**¹, SPE, National Energy Technology Laboratory; **Richard Hammack**, National Energy Technology Laboratory; **William Harbert**, University of Pittsburgh, National Energy Technology Laboratory

¹now with DiGioia Gray Inc.

Abstract

Hydraulic fracturing is a well-established technique to extract gas or liquid hydrocarbons from low-permeability formations like shale and tight gas reservoirs. Diffusion of hydrofracturing fluid outward from the stimulated fractures into the target formation produces slip across preexisting fractures and other discontinuities in the rock. Microseismic events recorded by downhole seismic monitoring arrays are a manifestation of associated deformation. Recent investigations suggest that the total cumulative seismic moment of microearthquakes during hydraulic fracturing is only a small portion of the total seismic energy release expected for the fluid volume injected into the formation. These observations suggest that other sources of energy release (such as inelastic deformation), contemporaneous with microseismicity, should be considered as relevant to the hydraulic fracturing process. Recent observations on long period, long duration (LPLD) seismic events suggest that slow slip emission along weaknesses that are misaligned with respect to the present-day stress field are likely an important mechanism of deformation and should be better understood and quantified in reservoir stimulations. In Morgantown, West Virginia, we carried out seismic monitoring of hydraulic fracturing activity using an array of five broadband, three-component surface seismometers. Using this network, we identified 89 high-amplitude, impulsive events and 436 long period, long duration (LPLD) events, with highly emergent waveform characteristics. In these interpreted LPLD events, we observed a significant concentration of energy in the 0.8-3 Hz frequency range. During hydraulic fracturing, LPLD events were found to occur most frequently when the pumping pressure and rate were at or near maximum values. As the main purpose of hydraulic fracturing is to stimulate oil and gas production from the less permeable reservoir, we compared the relative production contribution per stage to the frequency of occurrence of suspected LPLD events. We found positive correlation between the frequency of LPLD events and stage-by-stage gas production, highlighting the potential contribution of slow deformation processes and its effectiveness in the reservoir stimulation.

Introduction

Hydraulic fracturing of organic-rich shale and tight gas reservoirs is routinely performed to release hydrocarbons by opening hydraulic fractures and natural fractures within the formation. During hydraulic fracturing, large volumes of fluid are rapidly injected into the formation, which elevates the in-situ pore pressure thereby decreasing the effective pressure (the difference between confining and pore pressures). This change in effective pressure is usually strong enough to alter the stress stability of the rock within the injection zone. It first results into tensile opening of multiple new fractures in the immediate vicinity of the borehole that further interacts with the preexisting natural fractures of

variable orientation and increase the size, extent and hydraulic connectivity of preexisting fractures. The interaction between the hydraulic fracture and natural fractures depends on ambient stress, geomechanical properties of the rock, relative orientations of the natural fractures and the hydraulic fractures, rate of injection, etc. as further explained in Gu et al. (2011). The overall intent of hydraulic fracturing is to enhance the flow of oil and gas by increasing the interconnectivity of pore spaces, with its efficacy measured by the abundance and spatial distribution of microseismic events (Moos et al. 2011; Das and Zoback, 2013). For the most part, the correlation between the actual fraction of the rock volume that is stimulated during hydraulic fracturing and microseismicity is still not clear. This is an active area of research, with evidence both in support of and against the practice of using microseismicity as a proxy for the actual measure of stimulated reservoir volume (Wilson et al. 2016; Sicking et al. 2013).

A better understanding of a shale reservoir's response to hydraulic fracturing is needed to accurately estimate the volume of fractured/stimulated rock and to improve hydrocarbon production by more effective stimulation of the formation. The knowledge of a shale reservoir's response to stimulation can be used to optimize perforation spacing, number, and orientation; fracturing fluid composition; proppant size and loading; and fluid pumping schedules. However, even after the long use of hydraulic fracturing, beginning in the 1940s (Montgomery and Smith, 2010), the specific details of the stimulation mechanisms that drive the efficacy of hydraulic fracturing are still debatable. An energy budget for hydraulic fracturing that includes input and output energy components reveals a significant energy deficit in the occurrence of microseismic events when compared to the hydraulic work done by pumping fluid into the reservoir (Warpinski et al. 2012). Recent studies of Boroumand and Eaton (2012) and Kumar et al. (2017) have also highlighted the small contribution of energy (~20-25%) from microseismic (brittle failure mechanism) events. This suggests that estimates of stimulated reservoir volume (SRV) calculated using microseismic earthquakes alone is an underestimate of the true portion of the reservoir volume that is stimulated during hydraulic fracturing. Alternate deformation mechanisms in the reservoir rock during hydraulic fracturing should be included to improve the energy imbalance and to get more accurate estimates of the total stimulated reservoir volume.

Das and Zoback (2011) found evidence of low-frequency events in the Barnett Shale, between 10 and 80 Hz that persist for 10 to 100 seconds. In their analyses of microseismic data, acquired in the Eagle Ford Shale in NE Mexico, Hu et al. (2017) also found the presence of low frequency events during hydraulic fracturing, between 10 and 60 Hz, lasting for 30-60 seconds. In another study of the hydraulic fracturing of horizontal Marcellus Shale wells in southwestern Pennsylvania, Kumar et al. (2017) has also reported a similar type of low frequency events between 10 and 30 Hz. LPLD (long period long duration) events are low amplitude seismic phenomenon, characterized by emergent waveforms with no distinct P and S-wave arrivals, making phase picking difficult (Das and Zoback, 2011; Eaton et al. 2013; Kumar et al. 2016, 2017). High clay content (>30%) at a local scale, which increases shale ductility and promotes slow slip failure along fractures with a stable deformation rate, and slip along pre-existing fractures that are unfavorably oriented in the ambient stress field are two probable mechanisms for LPLD generation suggested in the literature (Das and Zoback, 2011; Zoback et al. 2012). In the case of LPLD events, analysis by Das and Zoback (2013) indicates that a large LPLD event represents an approximately 1000-fold increase in energy content over a microseismic event of moment magnitude $M_w \sim -2$. This difference in released

energy, between the LPLD event and the microseismic event, is likely due to the deformation of a fault of relatively larger size that can potentially contribute more to permeability enhancement during hydraulic fracturing, as suggested by Das and Zoback (2013).

In this study, we analyzed surface seismic data collected from a monitoring network of five 3C broadband seismometers during hydraulic fracturing of a total 58 stages in two horizontal Marcellus Shale wells in Monongalia County, West Virginia (**Fig. 1**). We examined the spectral characteristics of the recorded waveforms to characterize energy release at low seismic frequencies (0.8-3 Hz). During this analysis, we manually identified several long period events in the frequency range of 0.8-3 Hz that are temporally associated with hydraulic fracturing activity. These long period events and their waveform characteristics are similar to tectonic tremors and LPLD events previously reported from subduction zone environments and hydraulic fracturing operations in the Barnett and Marcellus Shale in Texas and southwestern Pennsylvania respectively (Shelly et al. 2006; Das & Zoback, 2011; Kumar et al. 2016, 2017). We observed elevated power of seismic energy in the 0.8-3 Hz frequency range in the spectrogram of individual LPLD events. Additionally, we also compared the production log data for individual stages from one of the horizontal wells with LPLD counts and various microseismic parameters to better understand their roles in reservoir stimulation and well productivity. We found a positive correlation between LPLD count and stage-by-stage gas production data (collected roughly one year after the hydraulic fracturing treatment), suggesting a definitive role of slow slip or non-brittle deformation in the reservoir stimulation.

Data and Method

We used a surface seismic network of five three component (3-C) broadband seismometers (Nanometrics-Trillium 120 Compact Posthole) to collect data during the hydraulic fracturing of two horizontal Marcellus Shale wells in Monongalia County, West Virginia (Fig. 1). We deployed the seismometers within 2 miles of the treatment well pad, with the nearest station (FRAC1) within 700 feet of the well pad. The approximate range of recording frequency for the broadband seismometer is 0.008-150 Hz, with a low noise floor, and it is highly sensitive to detect earthquakes from both local and regional seismicity. We optimized the geometry of the seismic network by placing seismometers around the northwest trending laterals (Fig. 1). Of the two laterals (MIP 3H and MIP 5H), well 5H was hydraulically fractured during October 28 – November 5, 2015 and well 3H during November 6 – 15, 2015. As summarized in **Table 1**, stages 1-6 of well 3H underwent geometric completion with fixed stage length and were pumped with a proppant of very fine sand size (100 mesh) at 35% volume percentage (procedure A in Table 1). The treatment condition of stages 7-12 only differed in proppant volume of fine sand (75%) from first six stages of well 3H (procedure B in Table 1). Stages 13-19 of well 3H were fractured using engineered completion design based on the geomechanical properties from the well logs run in the lateral (procedure C in Table 1) (Kavousi et al., 2017). The next two stages (stages 20-21) of well 3H were uniquely treated with engineered viscoelastic fluid and differed in this respect from all other stages that were fractured using slickwater fluid (procedure D in Table 1). The last seven stages (stages 22-28) of well 3H were fractured by combining engineered completion with various types of fracturing fluids. For well 5H, a uniform completion strategy (geometric completion with fixed stage length) was followed during the treatment of all 30 stages (**Table 2**). During hydraulic fracturing, the microseismic data was

collected using downhole string of 12 3-C geophones. In this study, we present our analysis of surface seismic data from three months of recording between September 2015 and November 2015.

While comparing the input and output energy during hydraulic fracturing operation, Boroumand and Eaton (2012) suggested three useful approaches to calculate the energy components (injection energy, fracture formation energy, and radiated seismic energy) involved in the brittle deformation and resulting microseismicity. Following the equation from Boroumand and Eaton (2012), we estimated the injection energy or total hydraulic energy input (E_{in} , in Joules) for 22 hydraulic fracturing stages at well 3H (the first 6 stages had no corresponding microseismic records) by using pumping rate (R , in ft^3/min), pumping pressure at the surface (P , in lb/ft^2) and total time duration (t , in minutes) of each stage:

$$E_{in}(\text{Joules}) = R(ft^3 / \text{min}) \cdot P(lb / ft^2) \cdot t(\text{min}) \cdot 1.356 \dots \dots \dots (1)$$

Here, the conversion factor 1.356 is used to convert the energy unit from ft-lb to Joules.

We estimate the fracture formation energy (energy required to create a fracture during the deformation process) for each stage following the mathematical equation of Boroumand and Eaton (2012):

$$E_f = P_d \cdot A_f \cdot w \cdot 1.356 \dots \dots \dots (2)$$

where E_f is the work done or energy (in Joules) required to create a tensile fracture of area A_f (ft^2) and width w (ft). P_d is the average downhole pressure that can be directly obtained from the operator or estimated from the surface pressure relationships. Further, Boroumand and Eaton (2012) suggested that fracture width (w) varying between 5-25 mm is wide enough to accept proppant. In this study, we used a conservative estimate of 5 mm wide fracture aperture. The product of height and length of the microseismic cloud is used as a proxy for the area of the hydraulic fracture (A_f) for each stage.

Lastly, we calculate the seismic energy released by all microearthquakes during a particular stage to quantify the portion of energy output that is contributed by microseismic events. We used the modified Kanamori's (1977) energy-moment relationship (Equation 3, below) as suggested by Boroumand and Eaton (2012) to calculate the radiated seismic energy for an individual microseismic event.

$$E_{out} = 10^{(1.5 \cdot M_w + 4.8)} \dots \dots \dots (3)$$

where E_{out} is the total output energy (in Joules) or released seismic energy (sum of P and S-wave energy) from each microseismic event and M_w is the moment magnitude of the microseismic event. We add the energy released of all microseismic events to get the estimate of cumulative energy released during the stage. Over the course of 22 out of the 28 fracturing stages of well 3H, we observed that the released energy (E_{out}) for all microseismic events during a particular stage and fracture formation energy (E_f) were significantly small compared to the total injection energy input (E_{in}). The sum of microseismic energy and fracture formation energy ($E_{out} + E_f$) was found to be varying in the range of 13-54% of the total injection energy (**Table 3**), with an average accountability of 30% (**Fig. 2**). During fracturing treatment, mechanical losses in the form of heat and frictional dissipation due to fluid transport through casing and perforations, and free flow of fluid into high secondary permeability zones can account for some of the energy deficit, but most likely it would not be enough to account for the total hydraulic energy input. This

deficit in the energy budget is in close agreement with the previous findings of Boroumand and Eaton (2012) that motivated the focus of our current study.

In our analysis, we removed the instrument response from the raw amplitude counts recorded by our surface seismometers to obtain the instrument corrected ground motion at each array station. For a preliminary search of low-frequency signals, we calculated the power spectral density (PSD) of ground acceleration as recorded by the surface seismometers. We selected 10 consecutive windows of 1 hour each, before and during fracturing of wells 5H and 3H, respectively, to estimate the PSDs of recorded ground motion for a cumulative time span of 20 hours for each well. We compared the power spectral density of the 10-hour windows before and during fluid injection for both stimulation phases (October and November 2015) as shown in **Fig. 3A** and **Fig. 3B**. In an exhaustive search for long duration events, we filtered the seismic waveform in frequency ranges of 1-30 Hz, 1-5 Hz and 0.8-3 Hz to remove the masking effect of high frequency signals and manually inspected the filtered data. We observed the clearest and best coherent signals between stations in the 0.8-3Hz-frequency band range. We initially identified 535 discrete events, with waveform characteristics typical of a suspected LPLD event, as discussed in Das and Zoback (2013). Each of these potential LPLD events is approximately 30-40 seconds in duration, with no impulsive P or S phase arrival and waveforms dominantly composed of S-wave arrivals. This larger contribution of energy from the S wave arrival is similar to the waveform characteristics of previously reported long duration seismic tremor in the subduction zone environment and LPLD events from the Barnett Shale, respectively (Shelly et al. 2006; Das & Zoback, 2013).

In our analyses of these suspected LPLD events, it was critical to rule out the possibility of misinterpreting regional or global earthquake-related waveforms as potential LPLD events. Regional earthquakes are a potential pitfall for the identification of LPLD events due to their overlapping frequency content and similar waveform characteristics, as pointed out in recent studies (Caffagni et al. 2015; Zecevic et al. 2016a, 2016b). We carefully examined the United States Geological Survey (USGS) earthquake catalog for reported seismicity during the time period of observed LPLD events and found temporal overlap with some small magnitude regional events within 1000 km radius of our study area (**Fig. 4**). We then checked the arrival time of individual LPLD events and did not find any temporal overlap with the expected arrival time of these small magnitude regional events within 1000 km radius. We also compared the temporal records of our observed LPLD events with the events reported in a larger search radius of 2000 km in the Advanced National Seismic System (ANSS) composite catalog. From our list of 535 events, we found temporal overlap with 22 events reported in the ANSS catalogs. This suggests that either the 513 events are small magnitude regional events below the detection threshold of standard catalogs or they are local events near our seismic network. To rule out the possibility of misidentifying small magnitude regional events as local earthquakes, we examined the waveform data from two stations of the nearby Central and Eastern United States Network (CEUSN), less than 70 miles from our study area (red pyramids, **Fig. 5**). Of 513 non-catalog events, we found temporal correlation with 77 events recorded by the CEUSN stations that we immediately discarded from our list of observed LPLD events. We calculated the spectrogram of the east-west component signal for our final list of 436 unique LPLDs that are missing from both regional catalogs and nearby stations of the US Array.

Zoback et al. (2012) suggested that long period events are likely associated with shear deformation along preexisting fractures of relatively larger size that may contribute more significantly to the stimulated reservoir volume (SRV) than conventional estimates based on microseismicity alone. Incorporating the contribution of LPLD seismicity into reservoir stimulation process may improve the estimates of producible oil and gas from unconventional reservoir, which is often assumed to be inherently related to the SRV associated with hydraulic fracturing stimulation (Warpinski et al. 2012). To quantify the effect of LPLD event occurrence on reservoir production potential, direct comparison of occurrence time of LPLD events with the well production data is the essential focus of our study. This was possible because in March 2017, a production log was run on horizontal Marcellus Shale well 3H to a measured depth of 13,580 feet. Measurements included 5 Mini-Spinners, 6 Water Holdup Measurements, 6 Gas Holdup Measurements, Relative Bearing, Deviation, Caliper, Pressure, and Temperature, recorded at various cable speeds during data collection. The goal of the production log was to resolve the contribution to total well flow from each of the perforated stage intervals and the fluid type contribution from those intervals. The acquisition of this high-quality production log presented the opportunity to compare gas production to the occurrence of LPLD events and various microseismic parameters, including cumulative moment, stress drop, source radius, seismogenic b-value, microseismic volume (estimated stimulated volume), and natural fracture density. We compared the time of occurrence of long period events observed during the hydraulic fracturing of well 3H and calculated microseismic parameters with the stage-by-stage production data to highlight their correlation with reservoir productivity. Gas production from each perforated stage of the well was documented as a percentage of the total production from the well. To facilitate ease of plotting multiple parameters on the same axis versus measured depth, all other parameters were also normalized to represent the contribution from each stage as a percentage of the total for the well. For example, LPLD count for each stage is shown as percentage rather than absolute number. Similar treatment was applied to b-value, cumulative seismic moment, source radius, stress drop, stimulated volume, and natural fracture density. In this way, relative increases and decreases in each parameter are directly comparable to each other.

While analyzing our records for LPLD events, we found some high amplitude discrete seismic arrivals with strongly impulsive waveform characteristics. Some of the impulsive events have waveform characteristics similar to explosions, mine roof collapses or mine blasts (all of these types of events display a pseudo-isotropic pressure pulse), with insignificant energy contribution from S-wave arrivals. We can pick P and S-arrivals for all other impulsive events on both the vertical and horizontal components. We used the absolute event location procedure in SEISAN (Havskov and Ottemoller, 1999) to locate a final list of 89 impulsive events, including 21 probable mine blasts. We also estimated their moment magnitude by utilizing the spectral parameters of displacement spectra in SEISAN.

Results and Discussions

The locations of high amplitude impulsive events are shown in Fig. 1. We observed two types of impulsive events with differing waveform characteristics. The two groups of events are geographically separated from each other and located on opposite ends of the two horizontal wells. The first group of events, located northwest of the horizontal wells, is composed of sparsely distributed hypocenters with waveform characteristics similar to a mine blast (green triangles in Fig. 1). The range of hypocentral depth varies between 0 and 3 km for the first group of events. We reviewed the USGS record of mined areas for the Pittsburgh coal bed in West Virginia (Ruppert et. al. 1996) and found an excellent spatial correlation between the location of these blast-type events and the southeastern edge of old underground mines in Monongalia County (grey shaded area in Fig. 1). This suggests that the impulsive events, having waveform signature similar to pseudo-isotropic pressure pulse, are perhaps related to roof collapse in the old mines or perhaps blasts associated with civil construction and surface mining activities.

Southeast of the horizontal wells, we located a second group of events (open circles in Fig. 1) with waveform characteristics similar to a natural earthquake. Events within the second group have hypocentral depth varying in the range of 0 to 22 km, with an average depth of 4.15 km. Their local magnitude (M_L) is found to be varying in the range of $M_L 0$ to $M_L 1.78$, with an average magnitude of 0.74. It forms a linear cluster of events, dominantly oriented north-south, with a minor extension in the northeast-southwest direction. We observed a decrease in event depth from north to south within the linear cluster of events. The northern half of the cluster is composed of deep crustal events with depth greater than 6.5 km, whereas events along the southern half are predominantly shallow crustal in origin with event depths less than equal to 3.5 km. We observed a subtle increase in hypocentral depth (~6.5km) for a small number of events along the eastern edge of southern half of the cluster. The deep crustal events in the northern half of the cluster are also characterized by relatively large magnitude events ($M_L \geq 0.8$) compared to shallow crustal and small magnitude earthquakes ($M_L \leq 0.8$) in the southern half. We do not observe any spatial overlap between the location of these normal earthquakes and horizontal Marcellus Shale wells. Many of the events from this distant cluster have less well-constrained hypocentral depth with large mean depth error (~25 km) that can be attributed to wide azimuthal gap (~360°, angle between two straight lines connecting an earthquake location with the two adjacent seismic stations in the network). We looked at the published literature for seismicity in central Appalachian (Bollinger 1969) to find the record of a specific geologic feature that can be correlated to our observed linear cluster of events. We are unable to find the evidence of any known crustal heterogeneity that can be readily associated with this north-south earthquake cluster. This linear cluster apparently coincides with the western flank of Chestnut Ridge anticline, the westernmost ridge in the Appalachian Plateau Physiographic Province (Fig. 1). We also found a class II injection well along the eastern edge of this earthquake cluster that is occasionally used for commercial brine disposal at ~8000 ft. (green star, Fig. 1). As widely evidenced in Central Oklahoma, underground disposal of saltwater could potentially increase the level of background seismicity (Walsh and Zoback, 2015). Considering the large error in hypocentral depth, it is difficult to quantify the exact nature of subsurface deformation related to this distant earthquake cluster. It is possible that the shallow events within this cluster are related to the subsurface variation in pore pressure resulting from brine disposal and deeper events are perhaps related to the tectonic deformation in the lower crust under this portion of Chestnut Ridge anticline in the Central Appalachians.

During hydraulic fracturing, we observed a significant increase in the power spectral density (PSD) between 7 and 30 Hz, with a larger number of peaks as compared to the pre-fracture time interval (Fig. 3). The difference in spectral peaks before and during the hydraulic fracturing is significant at three seismometer locations (FRAC1, FRAC2 and FRAC4) for both laterals (wells 5H and 3H). We observed a subtle difference in power spectral peaks for FRAC5 that can be attributed to greater loss of energy due to its distal location from the two horizontal Marcellus Shale wells. At FRAC3, data recording was discontinuous due to solar charging shortcomings and we are unable to calculate power spectra at the time when fracturing started. The increase in power spectral peaks during stimulation indicates a significant contribution of energy from the low frequency (<30 Hz) signal, with some minor differences in the frequency content of PSD peaks between the two wells (Figures 3A and 3B). As mentioned in the Method section, half of the time window used for power spectral analysis, spanned the first 10-hours during fracturing of both wells 5H and 3H. These 10-hour windows covered the fracturing interval of the first two stages of well 3H and the first stage of well 5H. As apparent in Tables 1 and 2, the treatment conditions of first two stages of well 3H differed from the first stage of well 5H in terms of total fluid, total proppant and average rate of injection although all three stages had the same treatment design. The differences in the PSD plot as observed in Figures 3A and 3B could be linked to different treatment parameters that affected local stress conditions and rock deformation characteristics leading to different ground motion and seismic emission of slightly differing frequency content.

Our detailed analyses of the filtered waveform in three different frequency range of 1-30Hz, 1-5 Hz and 0.8-3 Hz revealed large numbers of coherent signals in the 0.8-3 Hz frequency range. We looked at the spectrogram of discrete LPLD events recorded during the stimulation of wells 5H and 3H and found distinct flares of energy in the seismic frequency range between ~0.8 to 3 Hz for both wells, with occasional peaks continuing up to 4 Hz (**Fig. 6A** and **Fig. 6B**). Comparison of spectrograms recorded in this study with spectrograms recorded by Das and Zoback (2011) reveals similarity in the waveforms but a lower overall frequency content in our recordings. This difference in spectral content between previous studies and ours is perhaps an outcome of different positioning of the recording instruments. Das and Zoback (2011) used seismic data from the downhole geophone array while we used surface seismometers for spectral analyses. Placing geophones closer to the stimulated horizon would enable recording of higher frequencies that would otherwise be naturally filtered out along the path to a surface seismometer. Of the 436 LPLD events, 55% (242 events) of the LPLD events were identified during the stimulation of well 5H and 45% (194 events) during the hydraulic fracturing of well 3H. The difference in the number of recorded LPLD events during the stimulation of wells 3H and 5H is possibly linked to the different treatment strategies for these two wells. It is apparent from the analysis of Tables 1 and 2 that the hydraulic treatment strategies between wells 3H and 5H differed in the total number of fractured stages, injected volume of fluid, volume of proppant, and average rate of injection during their individual stages. Differences in hydraulic stimulation can potentially lead to the variation in local stress state during the fracturing of wells 3H and 5H, respectively. As the rock deformation characteristics during hydraulic fracturing strongly depends on the local stress condition in the subsurface, differences in the local stress state during the fracturing of wells 3H and 5H would result in corresponding changes in rock deformation behavior as well. The difference in microseismic response

(microseismic length, height, and volume; last three columns of Tables 1 and 2) of the fractured rocks between wells 3H and 5H is evidence of the effect of variable treatment conditions on the rock deformation behavior. Therefore, we think that the difference in the number of recorded LPLD events during the fracturing of wells 3H and 5H is a cumulative effect of the difference in various hydraulic treatment parameters during the fracturing of these two wells. Another possibility is the closer proximity of seismometers (FRAC2 and FRAC4) to well 5H, leading to improved detection for small magnitude LPLD events.

We carefully checked all available standard earthquake catalogs and data from nearby stations of CEUSN to avoid misinterpreting any small to large magnitude regional or distant events as potential LPLD events. From our final list of 436 LPLD events recorded during the stimulation of both wells (wells 5H and 3H), we selected some high quality LPLD events with high signal-to-noise ratio and analyzed 2-minute long records of CEUSN data spanning the arrival times of these selected LPLD events. We found no indication of small magnitude events during the relevant time intervals at both stations (O54A and Q54A) from CEUSN (**Fig. 7** and **Fig. 8**). It is apparent that the distant stations of CEUSN contain no corresponding records of LPLD events detected during the stimulation of wells 5H and 3H, both in time domain (panel 1 in **Figs. 7B-7C** and **Figs. 8B-8C**) as well as in frequency domain (panel 2 in **Figs. 7B-7C** and **Figs. 8B-8C**). The seismic waveforms recorded at both CEUSN stations appear to contain a uniform record of background noise, without any noticeable change in the amplitude level or frequency content with time. The absence of LPLD record from the CEUSN data is an important observation that likely suggests a local source of deformation for the causality of LPLD signal rather than small magnitude regional earthquakes not listed in the standard catalogs.

As suggested by Das and Zoback (2011) and Zoback et al. (2012), LPLD events during hydraulic fracturing are the result of significant increase in pore pressure that triggers shear deformation along sub-optimally oriented natural fractures. We therefore investigated temporal correlation between the time of occurrence of LPLD events and variation in the pumping parameters, such as pressure, rate, and proppant variation for the investigated hydrofracturing stages. It is noteworthy that well 3H underwent five different treatment procedures (A through E in Table 1) over the course of stimulation; whereas well 5H was stimulated using a single treatment strategy for all stages (Table 2). To capture the effect of the different treatment strategies used for well 3H, we selected five stages, one from each completion plan (variably colored in Table 1), and showed the occurrence of LPLD events during those five representative stages in **Fig. 9** (left column). We selected corresponding stages for well 5H to maintain consistency between the two wells (**Fig. 9**, right column). We noticed minor variations in LPLD event occurrence between treatment plans in well 3H and between the two wells, but LPLD events predominantly coincide with the time of increased pumping pressure and injection rate for both wells (**Fig. 9**). This is similar to the previous observation of Das and Zoback (2011) for the hydraulic fracturing of Barnett Shale and associated LPLD events. Our observed correlation between the time of occurrence of a majority of LPLD events and increased pumping pressure and rate is logical given that the maximum pore-pressure perturbation required to trigger slip along preexisting fractures is likely to correlate with the maximum pressure and rate. The minor differences observed among various stages and between the two wells could be linked to the difference in corresponding treatment

strategies (pump schedule, fluid content, proppant concentration, proppant size; summarized in Tables 1 and 2) and their local effect on rocks deformation characteristics.

Our attempt to find a correlation between gas production and the various observed seismogenic parameters reveals complex relationships contributing to well productivity (**Fig. 10** and **Fig. 11**). There are no highly correlated parameters, but stress drop, source radius (fracture area), seismic moment, and microseismic volume are the most highly correlated parameters at 37%, 42%, 40%, and 40% respectively (**Fig. 12A** and **Fig. 13**). The correlation with LPLD count is low, at only 14% (Fig. 13). This complicated relationship between stage-by-stage gas production and various parameters including microseismic parameters and LPLD count is perhaps linked with the differing completion procedures that were used for specific sets of fracturing stages of well 3H. Five different completion procedures were used that differed in perforation design, pump schedule, fluid content, proppant concentration and their size. As the response of the reservoir during hydraulic fracturing is a complex function of these components, any variation in them would result in a characteristic change in the geomechanical response of the reservoir. It is therefore likely that the observed complexity in the link between gas production and different treatment parameters is an outcome of the reservoir's complex response to different fracturing conditions. Another important aspect of our correlation between LPLD count and gas production, is the simple attribution of recorded tremors (LPLD events) to the specific stage being stimulated at the time. However, stimulation at any given stage may result in increased production from an adjacent stage, depending upon how fracturing fluids propagate away from the wellbore during stimulation. This possibility could partly explain the lesser correlation between LPLD count and stage-wise production data.

Of the 28 fracturing stages examined in this study, Stages 20 and 21 were fractured using an alternative viscoelastic fracturing fluid (VEF), specially engineered to increase well performance in shale reservoirs. Unfortunately, the gas production from individual perforations during these two alternative VEF stages was lower when compared to all other stages of well 3H, suggesting that the VEF fluid may not be appropriate for stimulating the Marcellus Shale reservoir. Therefore, the two stages using VEF fluid were excluded, and only stages using slickwater as the fracturing fluid were considered in the correlation between gas production and various seismogenic parameters. When we excluded stages 20 and 21 from the analysis, we observed a significant improvement in the relationship between LPLD count and gas production increased from 14% to 40% (Fig. 12B and Fig. 13), which is close to a three-fold improvement in the correlation coefficient, making LPLD an equally good predictor of production as other parameters (stress drop, source radius, seismic moment, and microseismic volume). The correlations of stress drop, source radius, seismic moment, and microseismic volume with production remain practically unchanged with the removal of stages 20 and 21 (Fig. 13).

Conclusions

In examining new three-component surface seismic data collected at a hydraulic fracturing site in Monongalia County, WV, we observed seismic events with waveforms characteristic of: 1) impulsive events with noticeable P and S-wave arrivals, and 2) emergent events, with no clear wave phases, which we interpret as Long Period, Long Duration (LPLD) seismogenic emissions. We found an excellent spatial correlation between coal mining areas and

impulsive events with waveform characteristics of pseudo-isotropic pressure pulse. These events are likely related to mine roof collapse and other mining related activities in the nearby region. We also noticed a linear cluster of impulsive events in Monongalia County that aligns with the western flank of Chestnut Ridge Anticline and is close to an intermittent wastewater disposal well. This distant cluster of seismic events is perhaps related to the reactivation of basement faults triggered by disposed fluids and/or small-scale crustal deformation in this tectonically complex portion of the Central Appalachians. Many of the seismic events observed in this study are similar to LPLD events previously documented in the Barnett Shale of Texas. We observed a noticeable difference in the power spectral peaks before and during hydraulic fracturing. This suggests a significant contribution of energy from the low frequency signal during stimulation. The spectral characteristics of low frequency events observed in this study are similar to observations in the Barnett Shale but with a lower overall frequency content in our recordings. The difference in spectral content between previous studies and ours is perhaps an outcome of different positioning of the recording instruments. While the Barnett study utilized a downhole acquisition system, we used surface seismometers for spectral analyses in this study. Placing geophones closer to the stimulated horizon would enable recording of higher frequencies that would otherwise be naturally filtered out along the path to a surface seismometer. For our final list of 436 unique LPLD events, we found no temporal overlap with any regionally reported events in the national earthquake catalogs and no corresponding waveform records in the nearby stations of CEUS network. The absence of temporal correlation between our observed LPLD events and regional earthquakes or data from the nearby seismic network suggests a local source of deformation for the occurrence of LPLD events as opposed to attenuated signals from known regional earthquakes of large magnitude or small magnitude events not listed in the standard catalogs. We observed correlation between LPLD occurrence and injection pressure and rate, with higher numbers of LPLDs generated at the maximum sustained stimulation pressure and rate, suggesting strongly that the highest pore pressure perturbations to the reservoir are responsible for LPLD generation. We also noticed a positive correlation between LPLD counts and the stage-by-stage gas production for one horizontal well where a production log was obtained. This finding suggests that the occurrence of LPLD events, an indicator of non-brittle deformation during hydraulic fracturing, may also be an indicator of reservoir stimulation and early gas production.

Disclaimer

This project was funded by the United States Department of Energy, National Energy Technology Laboratory, through a support contract with AECOM. Neither the United States Government nor any agency thereof, nor any of their employees, nor AECOM, nor any of their employees, makes any warranty, expressed or implied, or assumes any legal liability or responsibility for the accuracy, completeness, or usefulness of any information, apparatus, product, or process disclosed, or represents that its use would not infringe privately owned rights. Reference herein to any specific commercial product, process, or service by trade name, trademark, manufacturer, or otherwise, does not necessarily constitute or imply its endorsement, recommendation, or favoring by the United States Government or any agency thereof. The views and opinions of authors expressed herein do not necessarily state or reflect those of the United States Government or any agency thereof.

Acknowledgement

We are grateful to National Energy Technology Laboratory, Department of Energy for permission to publish this work. This research was supported by the National Energy Technology Laboratory's ongoing research under the RES contract DE-FE0004000. Special thanks to site operator Northeast Natural Energy for their permission to install seismometers in the vicinity of active well pad and for providing the microseismic and production data for this research. We would also like to acknowledge the National Science Foundation (NSF), United States Geological Survey (USGS), and Incorporated Research Institutions for Seismology (IRIS) for the seismic waveform data from Central and Eastern United States Network (CEUSN).

References

- Bollinger, G. A. 1969. Seismicity of the central Appalachian states of Virginia, West Virginia, and Maryland—1758 through 1968. *Bull. Seismol. Soc. Am.* **59** (5), 2103–2111.
- Boroumand, N. and Eaton, D. 2012. Comparing energy calculations - Hydraulic fracturing and microseismic monitoring. 74th EAGE Conference and Exhibition. Extended Abstracts, C042. <http://dx.doi.org/10.3997/2214-4609.20148187>.
- Caffagni, E., Eaton, D., van der Baan, M. et al. 2015. Regional seismicity: A potential pitfall for identification of long-period long-duration events. *Geophysics* **80** (1): A1-A5. <http://dx.doi.org/10.1190/geo2014-0382.1>.
- Das, I. and Zoback, M. D. 2011. Long period long duration seismic events during hydraulic fracture stimulation of a shale gas reservoir. *The Leading Edge* **30** (7): 778–786. <https://doi.org/10.1190/1.3609093>.
- Das, I. and Zoback, M.D. 2013. Long-period, long-duration seismic events during hydraulic stimulation of shale and tight-gas reservoirs—Part 1: Waveform characteristics. *Geophysics* **78** (6): KS97–KS108. <http://dx.doi.org/10.1190/geo2013-0164.1>.
- Eaton, D., van der Baan, M., Tary, B. et al. 2013. Broadband microseismic observations from a Montney hydraulic fracture treatment, northeastern British Columbia. *CSEG Recorder* **38** (3): 45–53.
- Gu, H., Weng, X., Lund, J. et al. 2011. Hydraulic fracture crossing natural fracture at non-orthogonal angles: A criterion, its validation and applications. SPE Hydraulic Fracturing Conference and Exhibition. 24-26 January. Woodlands, Texas, USA. Paper SPE-139984-MS. <https://doi.org/10.2118/139984-MS>.
- Havskov, J. and Ottemoller, L. 1999. SeisAn Earthquake Analysis Software. *Seism. Res. Lett.* **70**: 532-534. <http://dx.doi.org/10.1785/gssrl.70.5.532>.

Hu, H., Li, A., and Zavala-Torres, R. 2017. Long-period long-duration seismic events during hydraulic fracturing: Implications for tensile fracture development. *Geophys. Res. Lett.* **44** (10): 4814-4819. <http://dx.doi.org/10.1002/2017GL073582>.

Kanamori, H. 1977. The energy release in great earthquakes. *J. Geophys. Res.* **82**: 2981-2987. <http://dx.doi.org/10.1029/JB082i020p02981>.

Kavousi, P., Carr, T., Wilson, T. et al. 2017. Correlating distributed acoustic sensing (DAS) to natural fracture intensity for the Marcellus Shale. SEG International Exposition and Annual Meeting. 24-29 September, Houston, Texas, USA. Paper SEG-2017-17675576.

Kumar, A., Zorn, E., Hammack, R. et al. 2016. Surface seismic monitoring of hydraulic fracturing activity in Pennsylvania and West Virginia. Unconventional Resources Technology Conference, 1-3 August 2016, San Antonio, Texas, USA. 2435574. <https://doi.org/10.15530/urtec-2016-2435574>.

Kumar, A., Zorn, E., Hammack, R. et al. 2017. Long-period, long-duration seismicity observed during hydraulic fracturing of the Marcellus Shale in Greene County, Pennsylvania. *The Leading Edge* **36** (7): 580-587. <https://doi.org/10.1190/tle36070580.1>.

Montgomery, C. T. and Smith, M.B. 2010. Hydraulic fracturing: History of an enduring technology. *J. Pet. Technol.* **62** (12): 26-32. <http://dx.doi.org/10.2118/1210-0026-JPT>.

Moos, D., Vassilellis, G., Cade, R. et al. 2011. Predicting shale reservoir response to stimulation in the upper Devonian of West Virginia. SPE Annual Technical Conference and Exhibition. 30 October–2 November 2011, Denver, Colorado, USA. Paper SPE-145849-MS. <http://dx.doi.org/10.2118/145849-MS>.

Ruppert, L.F., Tewalt, S.J., Bragg, L.J. et al. 1996. Areal extent of the Pittsburgh coal bed and horizon and mines areas of the Pittsburgh coal bed. United States Geological Survey Open File Report 96-280.

Shelly, D. R., Beroza, G. C., Ide, S. et al. 2006. Low-frequency earthquakes in Shikoku, Japan, and their relationship to episodic tremor and slip. *Nature* **442**: 188–191. <http://dx.doi.org/10.1038/nature04931>.

Sicking, C., Vermiliye, J., Geiser, P. et al. 2013. Permeability field imaging from microseismic. *Geophysical Society of Houston Journal* **3**: 11–14. <http://dx.doi.org/10.1190/segam2012-1383.1>.

Walsh, F. and Zoback, M. D. 2015. Oklahoma's recent earthquakes and saltwater disposal. *Sci. Adv.* **1** (5), e1500195. <http://dx.doi.org/10.1126/sciadv.1500195>.

Warpinski, N. R., Du, J., and Zimmer, U. 2012. Measurements of hydraulic-fracture-induced seismicity in gas shales. SPE Hydraulic Fracturing Technology Conference. 6-8 February 2012, Woodlands, Texas, USA. Paper SPE-151597-PA. <http://dx.doi.org/10.2118/151597-PA>.

Wilson, T., Hart, A., and Sullivan, P. 2016. Interrelationships of Marcellus Shale gas production to frac-induced microseismicity, interpreted minor faults and fractures zones, and stimulated reservoir volume, Greene County, Pennsylvania. *Interpretation* **4**: T15-T30. <http://dx.doi.org/10.1190/INT-2015-0045.1>.

Zecevic, M., Daniel, G., and Jurick, D. 2016a. Questioning the Existence of Hydraulic Fracturing-Induced LPLD Events in a Barnett Shale, Texas, Microseismic Dataset. Sixth EAGE Workshop on Passive Seismic, Extended Abstracts. <http://dx.doi.org/10.3997/2214-4609.201600004>.

Zecevic, M., Daniel, G., and Jurick, D. 2016b. On the nature of long-period long-duration seismic events detected during hydraulic fracturing. *Geophysics* **81** (3): KS113-KS121. <http://dx.doi.org/10.1190/geo2015-0524.1>.

Zoback, M. D., Kohli, A., and Das, I. et al. 2012. The importance of slow slip on faults during hydraulic fracturing stimulation of shale gas reservoirs. SPE Americas Unconventional Resources Conference, 5-7 June 2012, Pittsburgh, Pennsylvania, USA. Paper SPE-155476-MS. <http://dx.doi.org/10.2118/155476-MS>.

Author Biographies

Abhash Kumar is a geophysicist at AECOM, a site support contractor for NETL. In this capacity since July 2016, he focuses on developing an improved understanding of the reservoir deformation mechanisms resulting from high-pressure fluid injection at various hydraulic fracturing and enhanced oil recovery/carbon sequestration sites. For his analysis, he uses passive seismic data collected using broadband seismometers to look at the seismic signals, recorded in various frequency bands. From 2015-2016, he was a post-doctoral researcher at NETL and worked on the low frequency seismic signals observed during the hydraulic fracturing of Marcellus Shale in Pennsylvania and West Virginia. His graduate work focused on seismotectonic studies of continental-scale mountain ranges to quantify the effect of deep lithospheric processes in the crust and upper mantle on seismic wave attenuation and evolutionary history of mountain ranges. Kumar is the author/coauthor of various research articles published in the peer-reviewed journals as well as conference proceedings. Kumar holds BS and M.Tech degrees in geology from India and a PhD in seismology from the University of North Carolina at Chapel Hill.

Erich Zorn is a senior geologist and Project Manager at DiGioia Gray, Inc. in Pittsburgh, Pennsylvania. In this capacity from July 2017, he is managing geological, geotechnical and aerial investigation projects for engineering applications. From 2016-2017, he was a post-doctoral researcher on Richard Hammack's team at the National Energy Technology Laboratory (NETL) in Pittsburgh, Pennsylvania. From 2005 – 2012, Zorn worked in the civil

and geotechnical engineering fields as a project geologist and a field team leader on major infrastructure projects. He returned to university in 2012 to pursue a PhD in geoscience with a focus on the oil and gas industry. During the summers of 2014 and 2015, Zorn completed internships at Chevron ETC in Houston, working on the Reservoir Properties from Seismic teams, where he concentrated on modelling the effects of fractures on seismic amplitudes. His PhD and post-doctoral work, both sponsored by NETL, focus on maximizing our understanding of reservoir properties through advanced analysis and interpretation of microseismic datasets acquired during hydraulic fracturing. Zorn has authored a small handful of publications, including a complimentary study to this one, based on data from central Pennsylvania. Other publications address topics such as the geotechnical challenges posed by deep excavations in claystone, and the instrumentation of excavations to detect slope instability during construction. Zorn holds BS, MS, and PhD degrees in geology from the University of Pittsburgh, Pennsylvania and is a licensed Professional Geologist in the state of Pennsylvania.

Richard Hammack leads the Monitoring Team in NETL's Office of Research and Innovation Center. In this capacity, he directs multidisciplinary field research pertaining to the safe and efficient development of domestic oil and gas resources and to the safe, permanent storage of CO₂ in underground reservoirs. Hammack's team partners with industry, state and federal agencies, and academia to answer questions that the public has about the safety and environmental impact of unconventional oil and gas development that uses multi-level horizontal drilling and hydraulic fracturing to release hydrocarbon resources from previously impermeable rock. In addition, Hammack's team is currently developing and demonstrating next generation geophysical tools to map CO₂ in the sequestering formation and provide frequent surveillance of underground drinking water sources for CO₂ and brine incursions. Prior to joining NETL, Hammack worked as a research geochemist for the U.S. Bureau of Mines where he developed methods for treating a wide variety of wastewaters from the mining, metallurgical, and oil and gas industries. In his early Bureau of Mines career, Hammack worked as an exploration geochemist and performed mineral assessments on Federal and Tribal Lands. He holds a BS degree in geology and an MS degree in geochemistry from the West Virginia University.

William Harbert is a Professor of geophysics at the University of Pittsburgh and an ORISE Research Associate at NETL. His interests are in petrophysics, geophysical reservoir surveillance, well log methods, electromagnetic and magnetic methods, geospatial analysis and geostatistics, and enhanced oil recovery using supercritical CO₂. He completed undergraduate degrees in Mathematics, Geology, and Geophysics, and holds an MS degree in exploration geophysics and a PhD in geophysics from Stanford University, followed by a post-doctoral appointment at the National Research Council (NRC). He has twice been the geology department chairperson, was the geophysics theme chair during the Pittsburgh AAPG International Meeting, the Society of Exploration Geophysicists District 4 Representative (elected), and Faculty Fellow in the Honors College of the University of Pittsburgh.

Figures

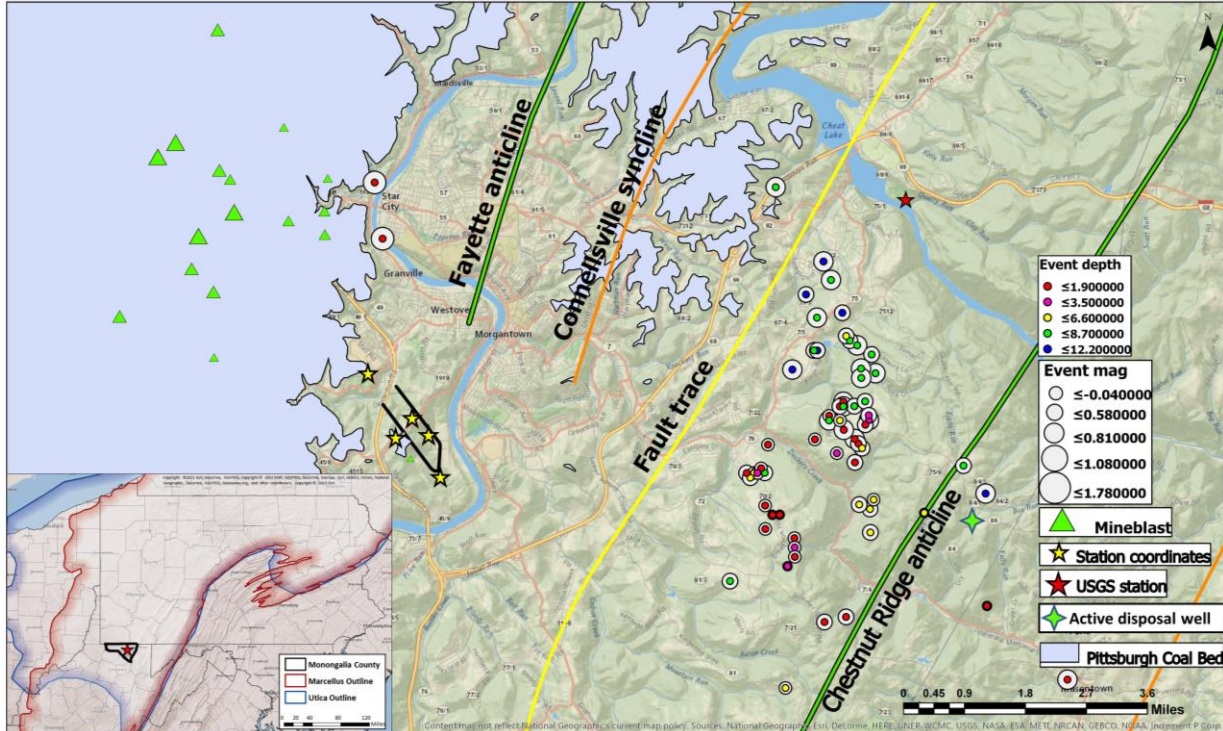


Fig. 1-Map showing the location of two horizontal wells (solid black lines) and five broadband seismometers (yellow stars) in Monongalia County, with a small inset in the bottom left showing the study area and outline of Marcellus Shale in West Virginia. Open circles represent the earthquake locations and the green triangles are mining or construction blasts located in the current study. Shaded grey area represents the outline of mined portion of the Pittsburgh Coalbed in Monongalia County, West Virginia.

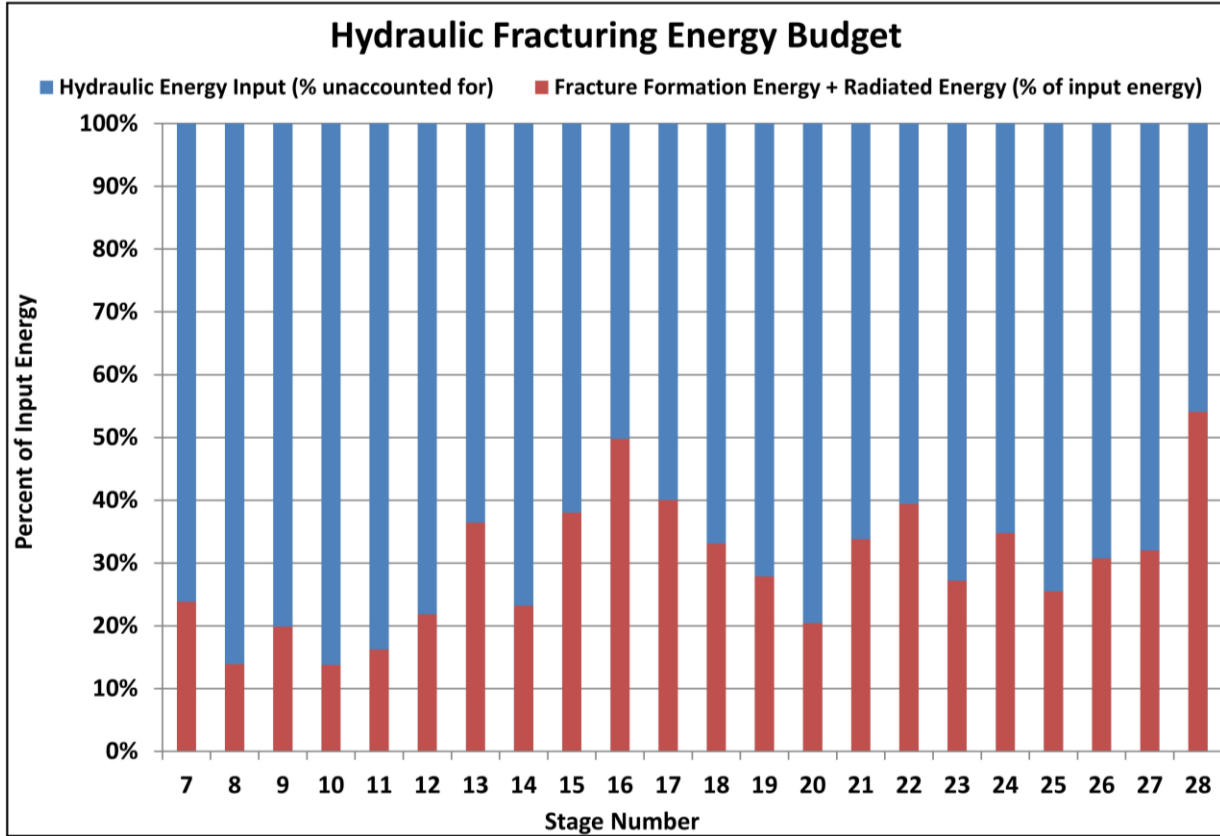


Fig. 2-Bar plot showing the estimates of hydraulic energy input and the sum of fracture formation energy and radiated microseismic energy for different stages in Well 3H.

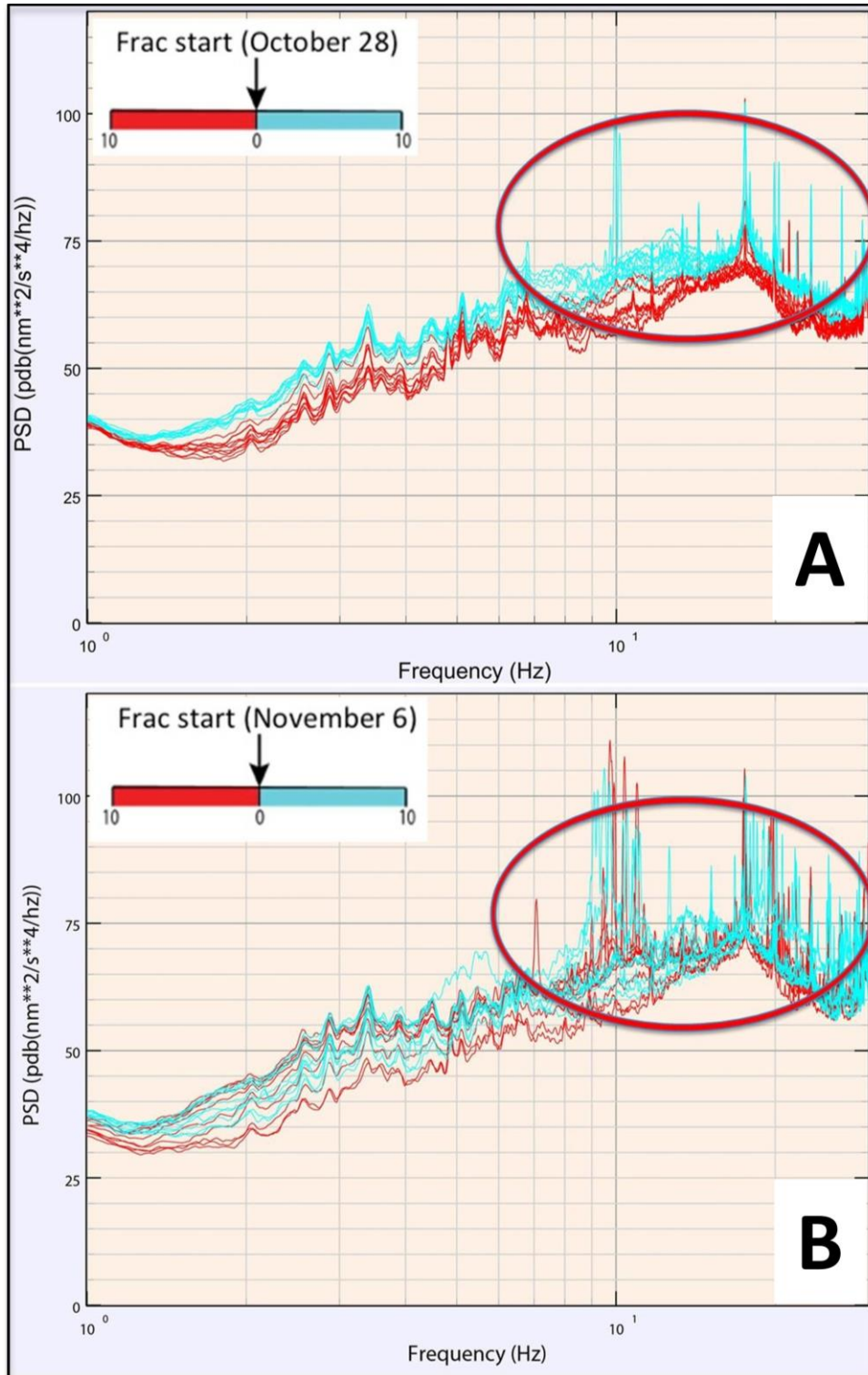


Fig. 3-Power spectral density (PSD) of ground acceleration before (red) and after (cyan) fracturing started on (A) October 28, 2015 for well 5H and (B) November 6, 2015 for well 3H. Here, pdb in the parenthesis of PSD (on y-axis) refers to power decibel, which by definition is proportional to $10 \log_{10}$ of the power (proportional to square) of a signal. In this case, signal refers to ground acceleration with unit (in nanometer) nm/s^2 and hence the unit of power decibel would be nm^2/s^4 . The frequency unit (hz) in the parenthesis of PSD (on y-axis) appears from the fact that PSD is mean power of the signal averaged over entire frequency spectrum.

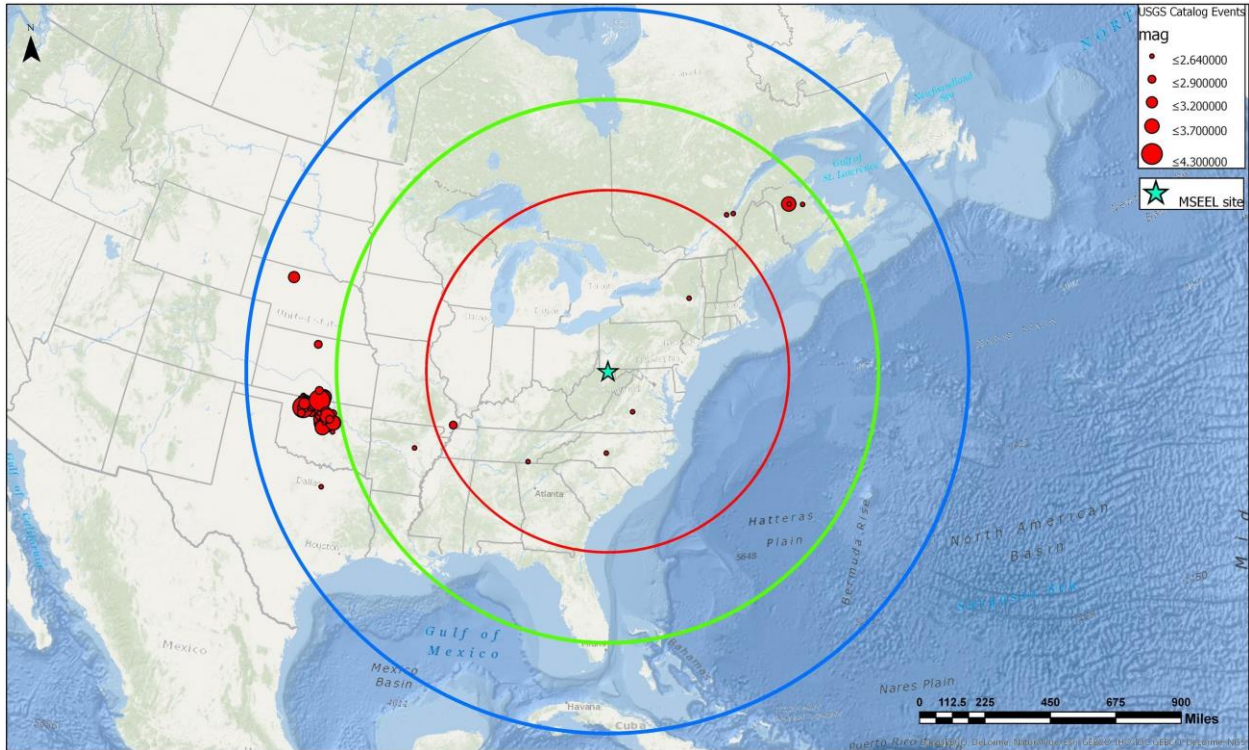


Fig. 4-Map showing the location of regional events (solid red dots) reported in the USGS catalog during the fracturing of well 5H and 3H. The red, green and blue circles drawn on the map have a radius of 1000 km, 1500 km, and 2000 km respectively. In the legend, MSEEL site refers to the Marcellus Shale Energy and Environment Laboratory site (location of the current study) in Monongalia County of West Virginia.

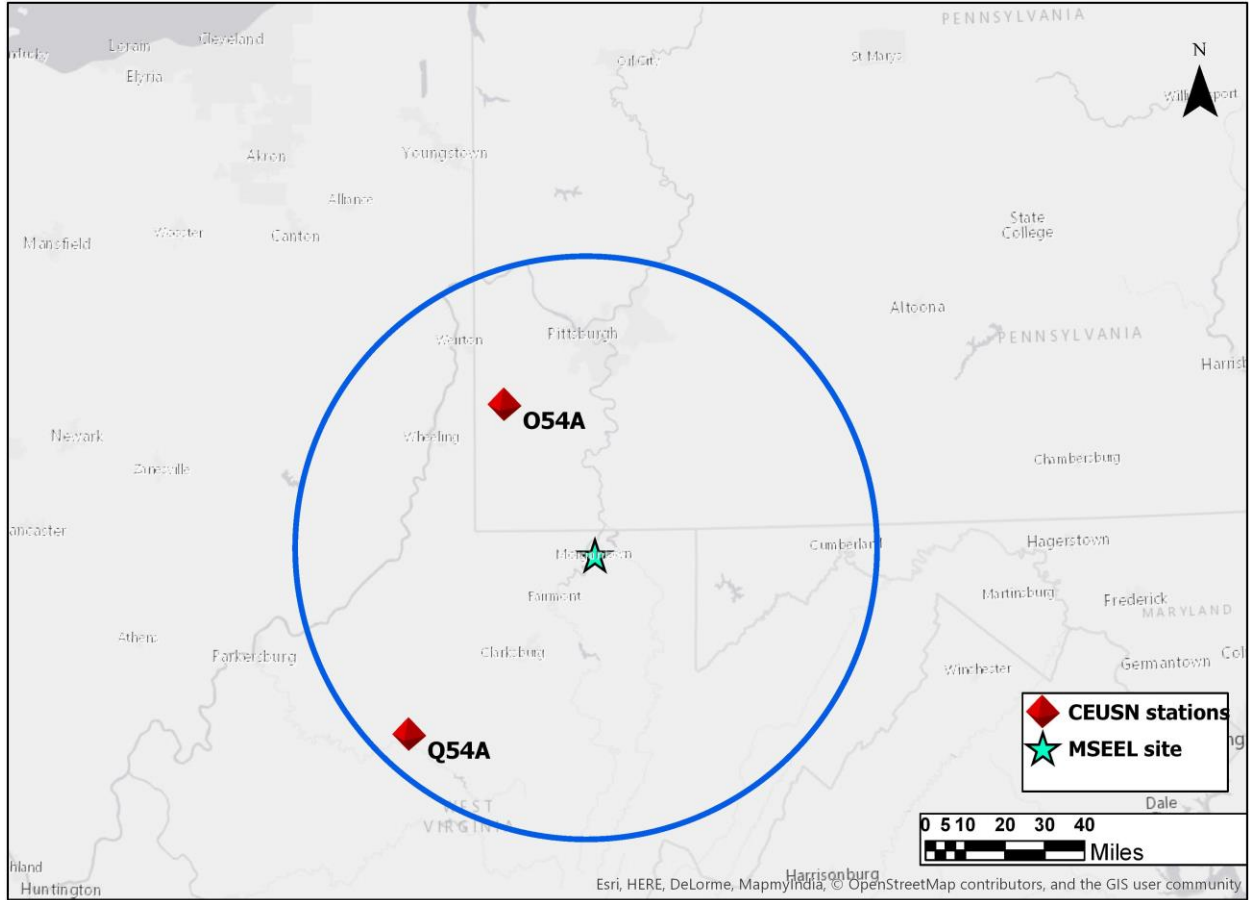


Fig. 5-Map showing the locations of nearby stations from Central and Eastern United States Network (red pyramids) used for waveform comparison with LPLD events recorded at Monongalia County site (cyan star). The circle (blue) drawn on the map has a radius of 70 miles.

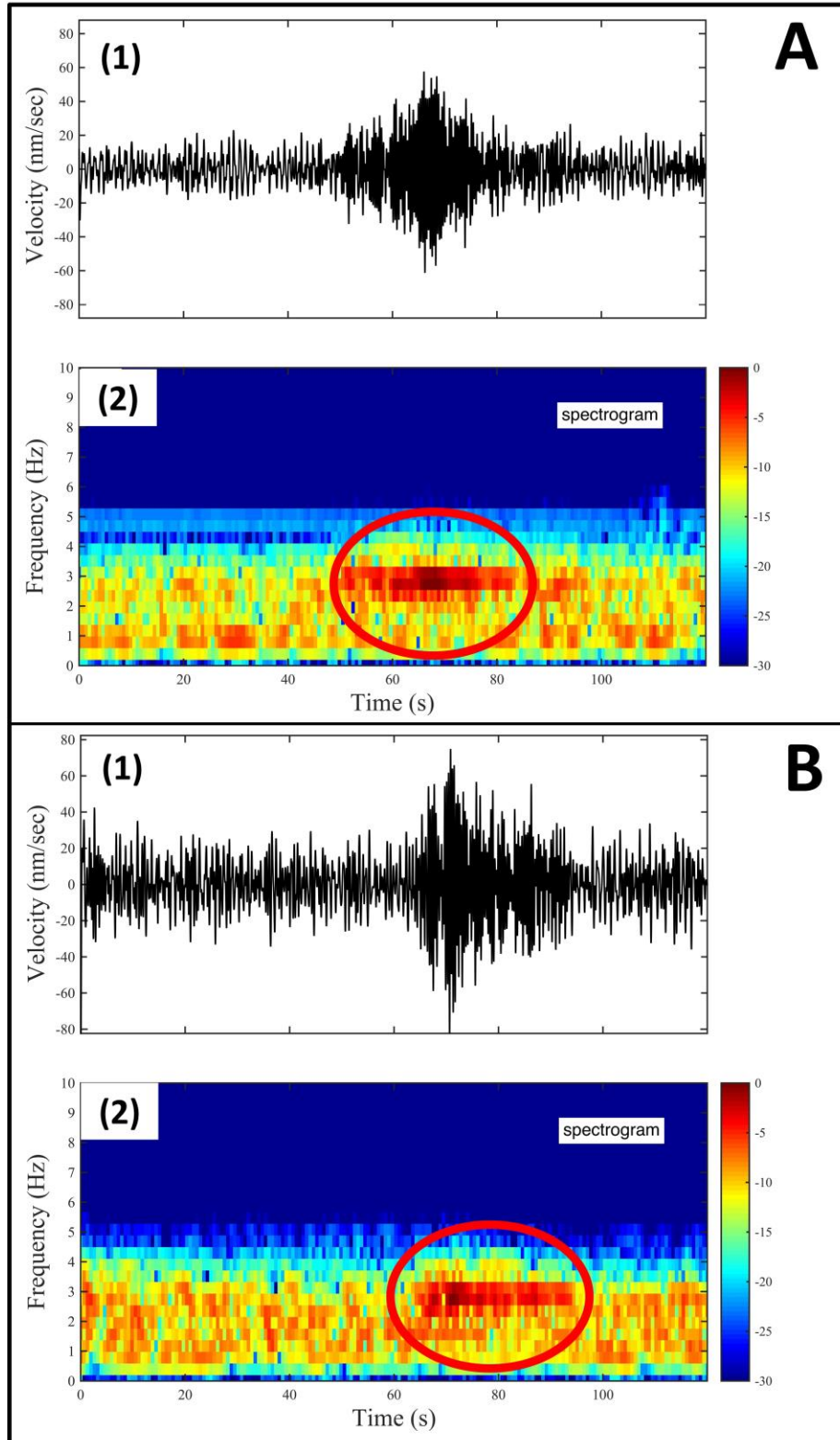


Fig. 6-Stacked waveforms (panel-1) and spectrograms (panel-2) of (A) a long duration event identified during October stimulation period of well 5H; (B) November stimulation period of well 3H. Color scale shows amplitude in decibels, with warmer colors corresponds to higher amplitude and vice-versa.

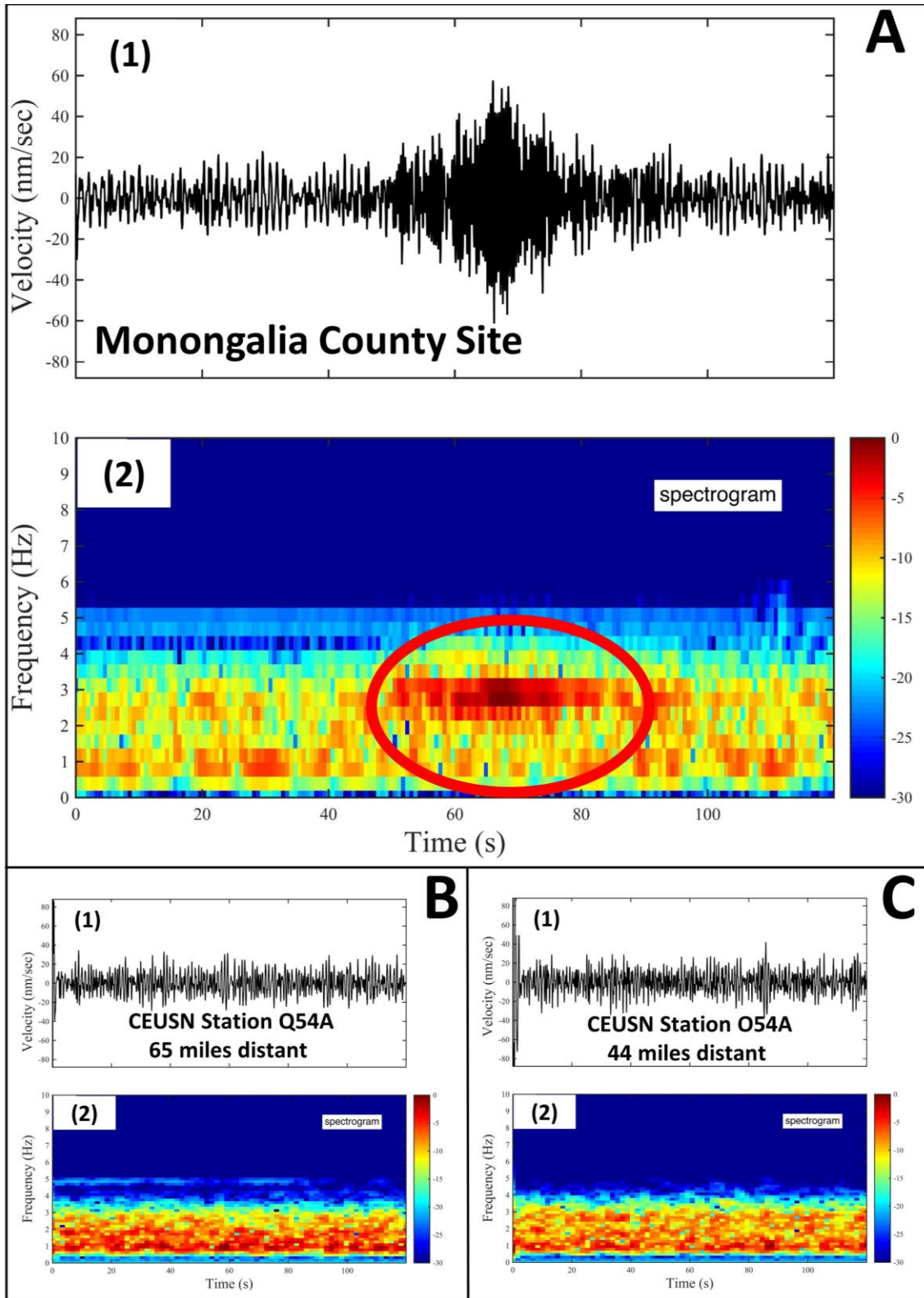


Fig. 7- Stacked seismic traces (panel 1) and spectrogram plots (panel 2) of (A) a long duration event recorded at MSEEL (Marcellus Shale Energy and Environment Laboratory) site from treatment well 5H; (B-C) Central and Eastern United States Network (CEUSN) data recorded at Q54A and O54A respectively for similar timeframe as used for panel A. The location of CEUSN stations is shown in Figure 5.

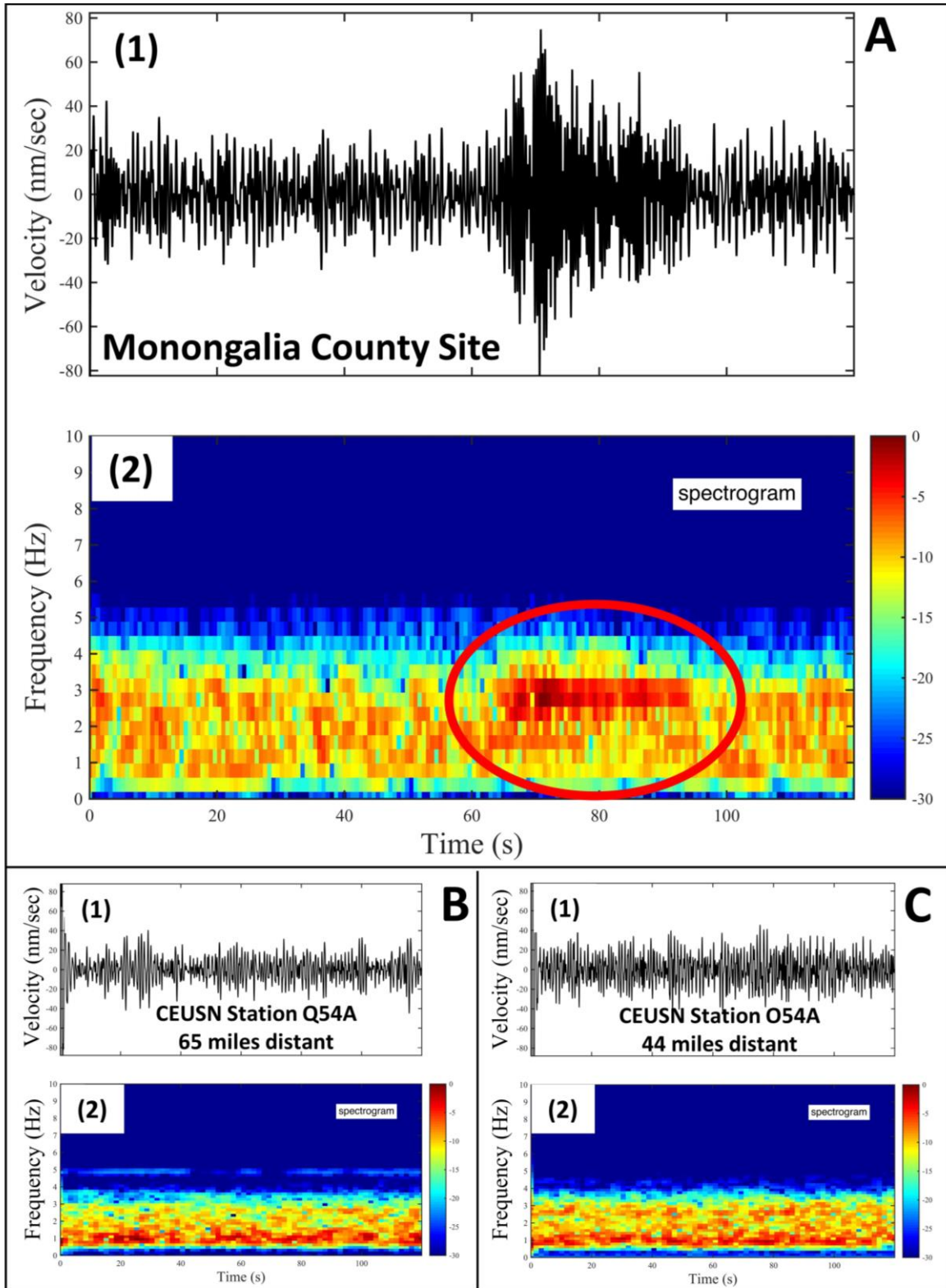


Fig. 8-Stacked seismic traces (panel 1) and spectrogram plots (panel 2) of (A) a long duration event recorded at MSEEL (Marcellus Shale Energy and Environment Laboratory) site from treatment well 3H; (B-C) Central and Eastern United States Network (CEUSN) data recorded at Q54A and O54A respectively for similar timeframe as used for panel A. The location of CEUSN stations is shown in Figure 5.

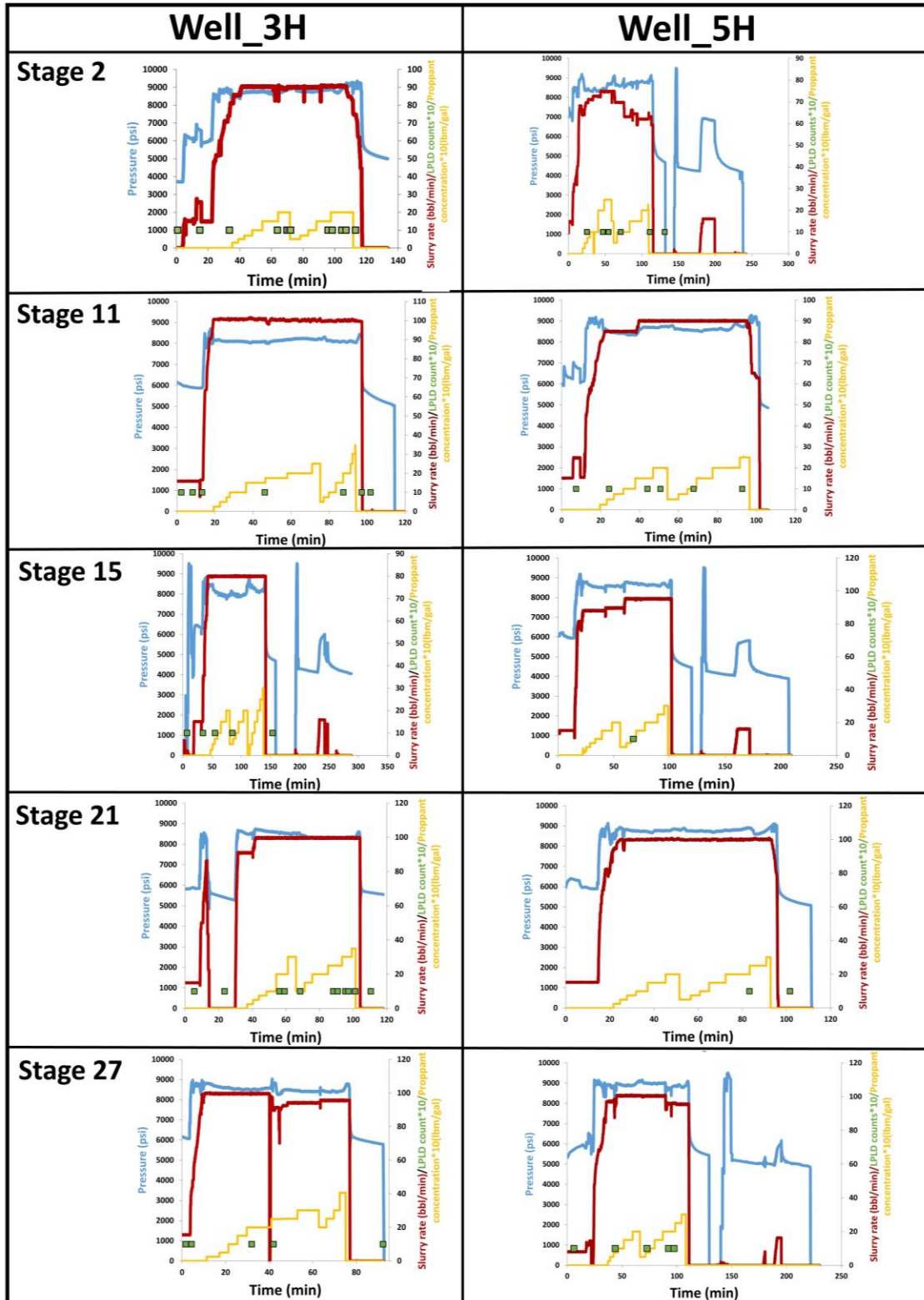


Fig. 9-Comparison between frequency of occurrence of LPLD events and injection parameters for representative stages of well 3H (left column) and 5H (right column). Long duration events are shown as green rectangles for stages 2, 11, 15, 21, and 27 of wells 3H and 5H, with solid lines representing surface pressure recording (blue), slurry rate (red), and proppant concentration (yellow). Common stages are shown for wells 3H and 5H in the left and right column, respectively.

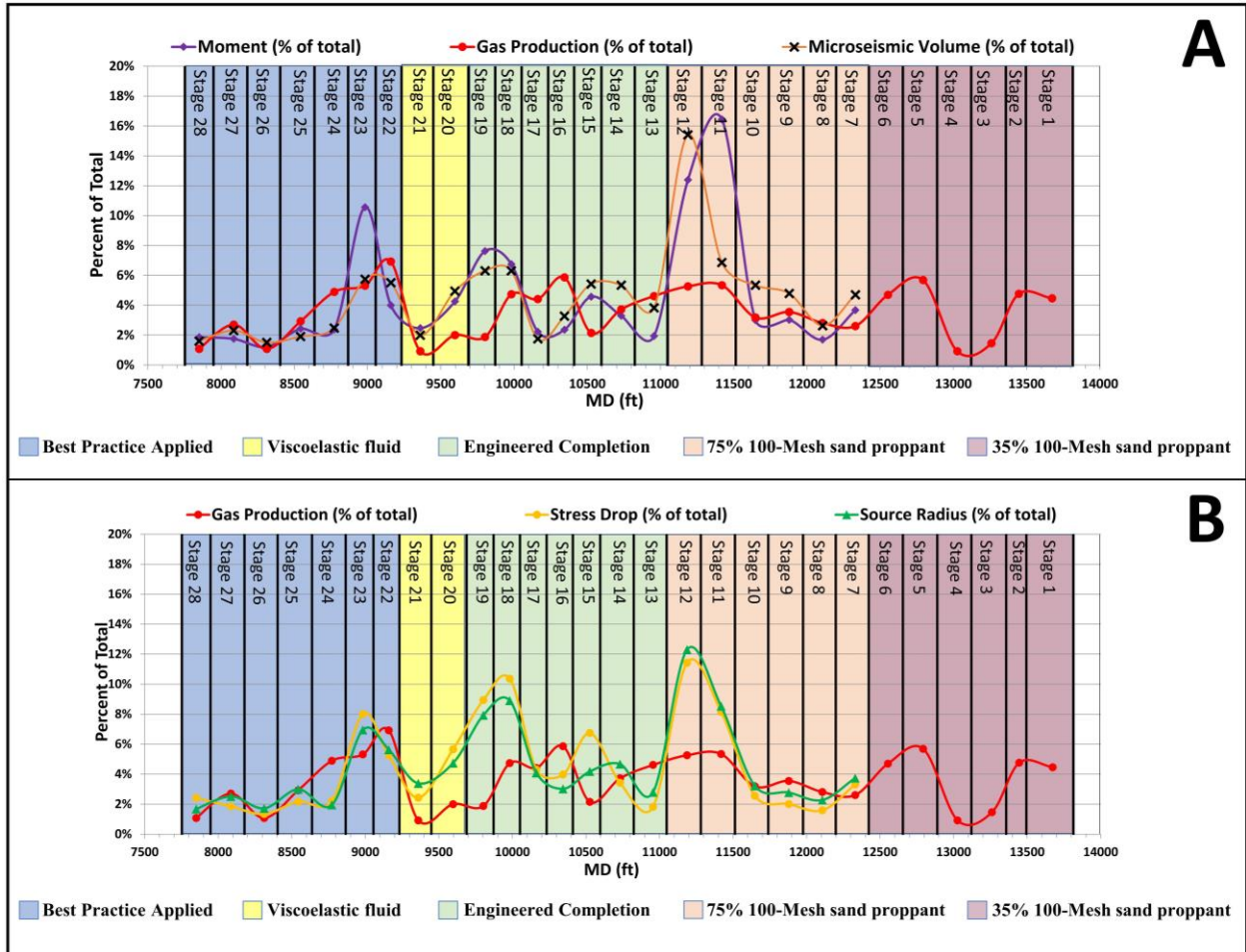


Fig. 10-Comparison between relative production contributions per stage (red curve) from well 3H to the (A) cumulative seismic moment (purple curve) and microseismic volume (brown curve); (B) stress drop (yellow curve) and microseismic source radius (green curve). The background colors represents five different completion procedures as shown by legends at the bottom.

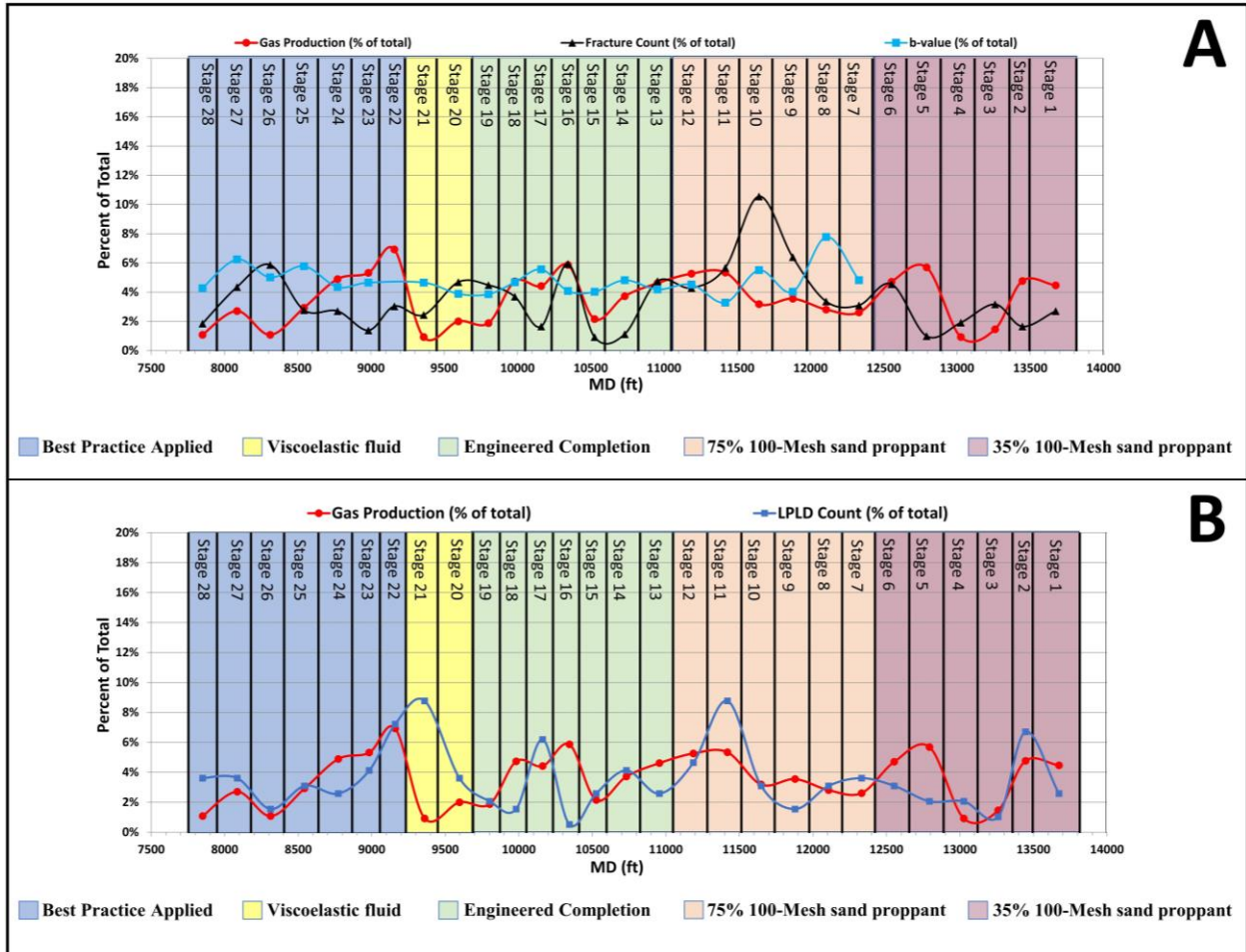


Fig. 11- Comparison between relative production contributions per stage (red curve) from well 3H to the (A) fracture count (black curve) and b-value (blue curve); (B) frequency of occurrence of observed LPLD events (blue curve). The background colors have similar significance as in Figure 10.

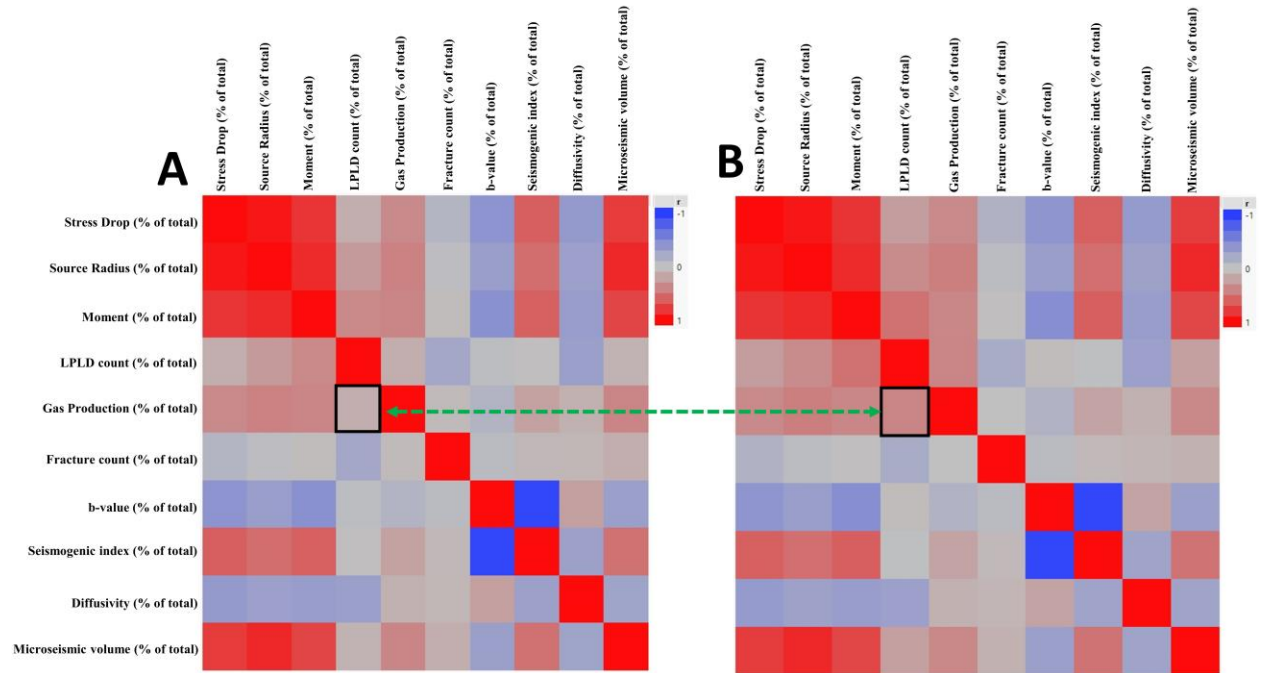


Fig. 12-2-D plot of cross correlation matrix showing parameter correlation for (A) all 28 stages included (B) excluding stages 20 and 21 for Well 3H. Two rectangular boxes highlighted in black represent the correlation between LPLD count and stage-by-stage gas production for all 28 stages included (left) and excluding stages 20 and 21 (right).

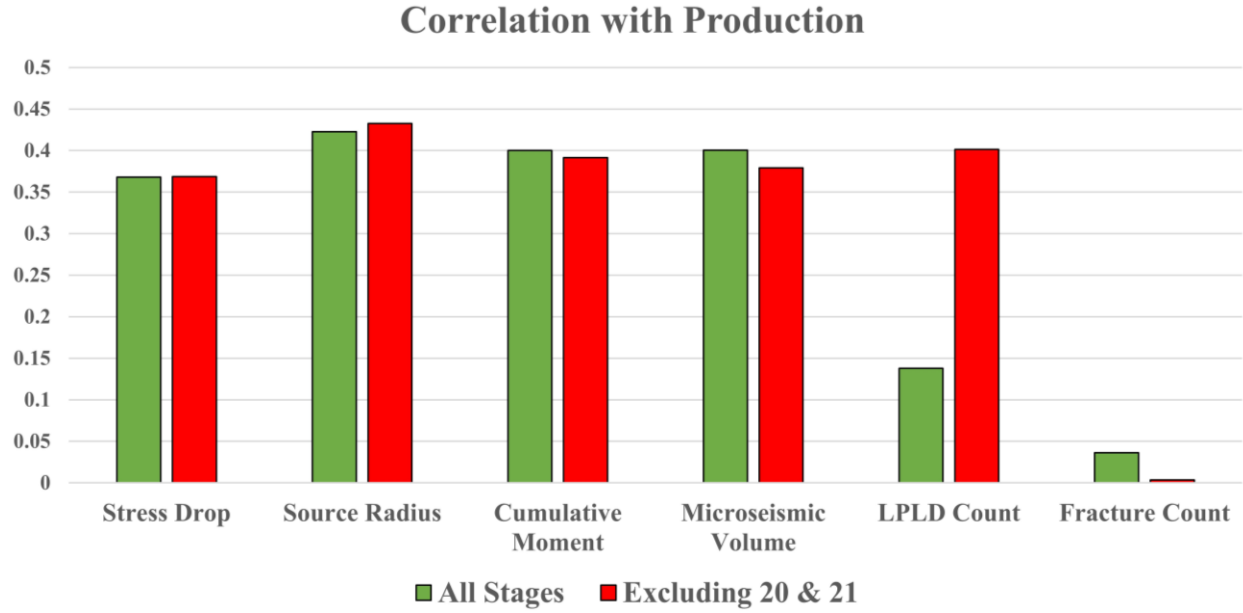


Fig. 13-Bar plot showing the comparison of cross correlation of different parameters with production for all stages included (green bars) and excluding stages 20 and 21 (red bar).

Table 1. Hydraulic stimulation execution summary with microseismic evaluation results for 28 stages of well 3H. Five different completion procedures (A through E) are color-coded to maintain the consistency with Figures 10 and 11.

Completion procedure	Stage number	Total fluid (1000_gal)	Total proppant (1000_lbm)	Average rate (bbl/min)	Total microseismic length (ft)	Total microseismic height (ft)	Microseismic volume (million ft ³)
A (Geometric completion with scheduled pumping of 35% sand proppant of 100 mesh size)	Stage 1	448	420	81.8	N/A	N/A	N/A
	Stage 2	332	346	88.4	N/A	N/A	N/A
	Stage 3	368	399	85	N/A	N/A	N/A
	Stage 4	383	440	90	N/A	N/A	N/A
	Stage 5	307.8	349	88.5	N/A	N/A	N/A
	Stage 6	400.8	440.1	89.3	N/A	N/A	N/A
B (Geometric completion with scheduled pumping of 75% sand proppant of 100 mesh size)	Stage 7	386.9	440.9	87.1	1387	512	5.9
	Stage 8	368.5	440.5	95	1097	387	3.3
	Stage 9	365.3	441	98.6	1156	545	6
	Stage 10	353.1	440	100	1250	335	6.7
	Stage 11	338.2	440.5	99.9	1233	378	8.6
	Stage 12	377.3	440.7	99.2	1453	480	19.3
C (Engineered completion with variable stage length and treatment parameters)	Stage 13	313.6	360.3	95.1	1924	516	4.8
	Stage 14	369.4	437.1	98.3	1227	500	6.7
	Stage 15	344.7	360	79.9	1510	723	6.8
	Stage 16	257.8	188.5	77.8	1575	711	4.1
	Stage 17	293.2	351.1	79.4	1189	658	2.2
	Stage 18	290	291.9	92.4	1496	516	7.9
D (Engineered viscoelastic fluid)	Stage 19	327.9	360.7	98.8	1552	507	7.9
	Stage 20	314.8	439.3	96.7	1472	395	6.2
E (Variable treatment strategies applied by the operator)	Stage 21	305.7	440.6	94.6	1508	534	2.5
	Stage 22	452.7	437.7	93.3	1576	492	6.9
	Stage 23	363.2	436.1	99.8	1602	516	7.2
	Stage 24	347.2	440.3	98.8	2403	410	3.1
	Stage 25	338.7	442.7	98.7	1679	419	2.4
	Stage 26	304.1	440.1	99.7	2055	478	1.9
	Stage 27	274.6	453.3	93.4	1662	482	2.9
	Stage 28	309.8	366	94.1	1372	1059	2

Table 2. Hydraulic stimulation execution summary with microseismic evaluation results for 30 stages of well 5H.

Completion procedure	Stage number	Total fluid (1000_gal)	Total proppant (1000_lbm)	Average rate (bbl/min)	Total microseismic length (ft)	Total microseismic height (ft)	Microseismic volume (million ft ³)
Geometric completion with scheduled pumping of 35% sand proppant of 100 mesh size	Stage 1	267.6	328.9	69.8	N/A	N/A	N/A
	Stage 2	290.4	329	68.5	1003	1101	7.9
	Stage 3	234.8	265.6	81.8	N/A	N/A	N/A
	Stage 4	220.6	260.5	77.4	N/A	N/A	N/A
	Stage 5	257.8	272.3	75.1	180	213	N/A
	Stage 6	326.3	267.4	87.5	1042	564	N/A
	Stage 7	358.6	401.5	78.8	1091	538	N/A
	Stage 8	323.4	400.2	81.2	1137	655	2.9
	Stage 9	317.4	398.6	84.7	790	743	N/A
	Stage 10	324.5	398.9	91.2	1565	957	2.6
	Stage 11	315.6	358.2	83.7	1204	727	5.9
	Stage 12	332.4	403.4	85.9	1147	678	4.7
	Stage 13	372.2	394.6	92.8	1447	1059	9.1
	Stage 14	325.7	400.1	92.7	1488	955	8.5
	Stage 15	322.3	403.2	93.7	1660	895	2.5
	Stage 16	306.1	347.1	89.6	1354	812	6
	Stage 17	328.5	400.5	90	1155	695	4.8
	Stage 18	323	397.2	88.7	1210	639	3.7
	Stage 19	325.7	400.5	93.9	1198	831	5.7
	Stage 20	313.5	378.6	94.4	1755	1124	1.6
	Stage 21	322.8	442.6	99.5	1516	823	2.5
	Stage 22	327.3	401.8	94.7	1419	965	1.9
	Stage 23	242.8	290.9	92.8	1294	888	3.9
	Stage 24	305	334.6	97.7	1186	439	1.1
	Stage 25	316.5	358.3	97.6	1121	841	2.1
	Stage 26	340	402.1	96.9	1349	1022	1.2
	Stage 27	336.6	398.8	93.9	1415	856	0.2
	Stage 28	351.3	394.8	91.2	1192	473	2.5
	Stage 29	337.2	399.7	99.6	773	662	4.1
	Stage 30	342	400.6	99.2	1334	567	6.2

Table 3. Energy components and their relative contribution during hydraulic fracturing of well 3H

Stage	Energy input (E_{in} _joules)	Microseismic Energy (E_{out} _joules)	Fracture energy (E_f _joules)	$(E_{out}+E_f)/E_{in} * 100$	Unaccounted energy (%)
7	77511677264	42810.01119	18476908275	24	76
8	85488111889	19858.7588	11872203003	14	86
9	89065146349	35207.11029	17697197528	20	80
10	78522387868	36198.89283	10797142406	14	86
11	73029299123	192673.9987	11845532755	16	84
12	81800579894	147646.9014	17869641009	22	78
13	74043440903	27410.72477	26972205798	36	64
14	71822926403	47395.90889	16663889120	23	77
15	72976209381	60920.6316	27733288528	38	62
16	60271897351	32786.67835	29993361839	50	50
17	49559476037	37317.38002	19832840348	40	60
18	62383615465	92966.62525	20646572070	33	67
19	75818087222	100260.1453	21112218712	28	72
20	73547191349	62322.16979	15022858597	20	80
21	62307055147	31664.93816	21045086161	34	66
22	49762479873	49935.8055	19595588715	39	61
23	80008017125	124374.8376	21740188186	27	73
24	75852831092	28211.43748	26354514209	35	65
25	73850867016	28863.19578	18813978702	25	75
26	84630957490	14550.74603	25999669908	31	69
27	66267264388	20989.82215	21195924058	32	68
28	69884714718	21517.62211	37785424643	54	46